NAVIER-STOKES ANALYSIS FOR SCT LOW-SPEED HIGH-LIFT FLIGHT AND WIND TUNNEL CONFIGURATIONS

Vincenzo Brandi
CIRA - Italian Aerospace Research Center
Via Maiorise, 81043, Capua (CE), Italy

Keywords: *vortex flow, SCT configuration, high-lift computations, WT model installation effect*

Abstract

This paper deals with the flow characteristics around the Supersonic Commercial Transport wing body and 1:22 wind tunnel model at typical flyover design conditions. These activities have been performed within the framework of EC-project EPISTLE. The configurations differ from each other in the inclusion of a underwing pylon in the wind tunnel model to offset the low-thickness wing bending. The flow field has been evaluated by solving the Reynolds-Averaged Navier-Stokes equations with the Kok TNT $\kappa - \omega$ *turbulence model. The numerical results are compared with measured data collected in the ONERA F1 wind tunnel. The wind tunnel model installation effect has been assessed by including the pylon in the computations.*

1 Introduction

The European Community (EC) funded EPISTLE (**E**uropean **P**roject for the **I**mprovement of **S**upersonic **T**ransport **L**ow speed **E**fficiency) project[6] ran from March 2000 to November 2003 during the 5th R&D Framework Program. It led to alternative designs for the *"new generation"* Supersonic Commercial Transport (SCT) nose-droop-like high-lift systems that exhibited higher aerodynamic efficiency at low-speed with respect to the preliminary *"datum"* configuration, Fig.1, that was developed during the previous EC funded EUROSUP project during the 4th R&D Framework Program[9]. EPISTLE partners were asked to validate their CFD tools on this configuration during the first part of the project in order to assess the code capabilities to predict separated flows within prescribed accuracy for the design validation phase[5]. CIRA's ZEN code[8] also demonstrated its capabilities to predict open separation flow at design point[1].

Alternative leading edge geometry were conceived during the design phase by the German Aerospace Center, DLR, acting on the hinge line position, and by Dutch Aerospace Center, NLR, acting on the double hinge line concept, both leading to extend attached flow on the wing.

During the design validation phase, the preliminary configuration visible in Fig.1 was replaced by a more realistic, closer to a *"flight"* one, with an upswept finite-length fuselage and a rounded wing tip, Fig.2.

A 1:22 scale modular model with the opportunity to accomodate different leading edges was built to assess the performance gain of the alternative designed high-lift systems over the datum one. Experimental data were collected during two different campaigns, the former held in September 2002, the latter in November/December 2002, both in the French Aerospace Center, ONERA, F1 wind tunnel at Fauga-Mauzac[4]. The first campaign was devoted to the collection of global aerodynamic coefficients and pressure data on all the three configurations. The second campaign was designed to collect more detailed data, namely on the boundary layer and in the wake, for the NLR design which exhibited the best performance dur-

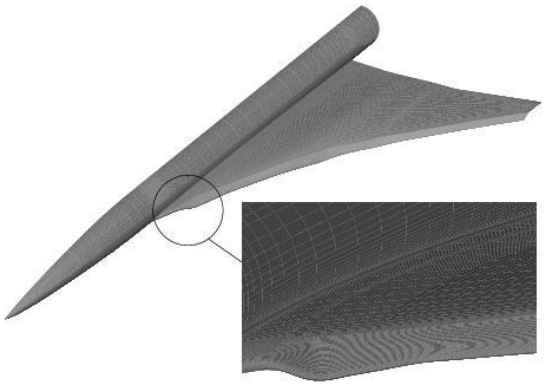

Fig. 1 Low-Speed High-Lift SCT Configuration as designed during the EUROSUP Project.

ing the first test. Fig.3 shows the model installation in the ONERA F1 wind tunnel.

An under-wing pylon was included in the wind tunnel model in order to stiffen the outer wing to offset wing tip bending due to the airfoils' low thickness. Such issue came up during the detailed design phase of the wind tunnel model[3]. Among EPISTLE partners, CIRA was asked to perform the aerodynamic analysis around the so-called *"wind tunnel configuration"* in which the under-wing pylon was modelled, Fig.4. The objective of this work is to provide the reference numerical aerodynamic solution on the *"datum"* configuration with an attempt to estimate the wind tunnel installation effect on the aerodynamic coefficients.

2 Grid generation around the *"datum"* wing body and wind tunnel configuration

A computational mesh was generated around the configuration without the sub-wing pylon, the so-called *"wing body configuration"*, by adapting the existing C-(C-C) topology generated for the EUROSUP *"datum"* configuration during the acceptance test exercise[1]. The computational domain approximately extends six semi-span in each directions and contains 121 blocks, Fig.5. The mesh size in the finer level is around 4 millions of cells. Two sub-levels could be drawn, a coarse level with 61799 cells and a medium level with 494392 cells.

Later on, a local topology modification, Fig.6, has been performed to include the sub-wing pylon to obtain the *"wind tunnel configuration"* computational grid with 137 blocks and around 4.3 millions of cells.

3 Flow condition of numerical analysis

CIRA has applied the Reynolds-Averaged Navier-Stokes (RANS) flow solver ZEN[8] to compute the aerodynamic flow field around the SCT *"datum"* configuration.

All the calculations have been performed

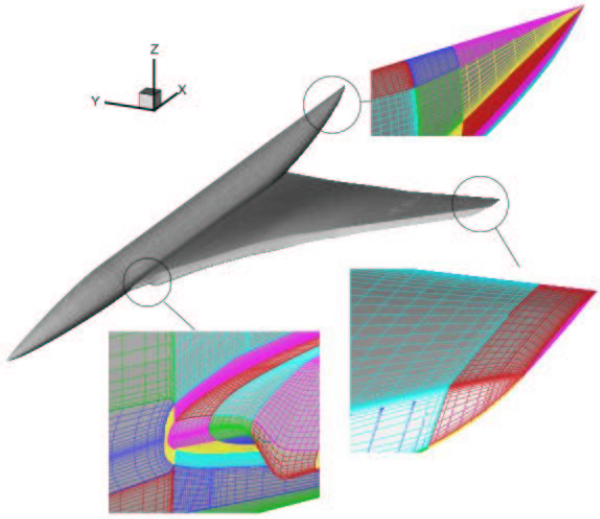

Fig. 2 EPISTLE validation phase configuration: Detail of Geometric Variants with respect the EUROSUP Configuration of Fig.1.

Fig. 3 EPISTLE Model Installation in the ONERA F1 Wind Tunnel.

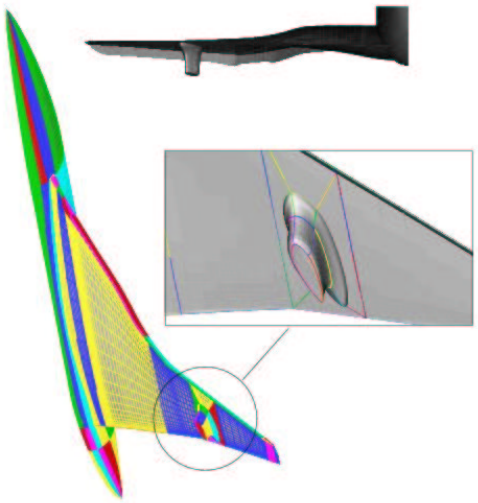

Fig. 4 Wind Tunnel Configuration with the Pylon on the Wing Lower Surface.

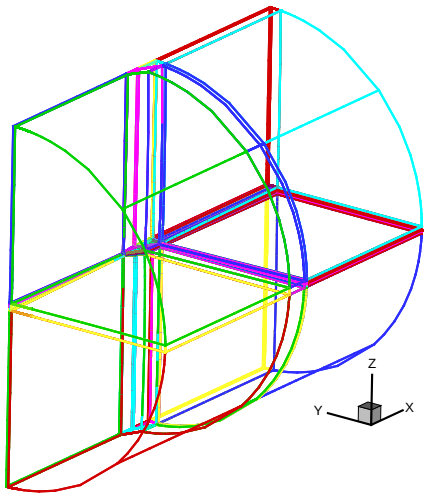

Fig. 5 The Domain Decomposition of the CIRA Grid with 121 Blocks.

at Mach number 0.25 and at Reynolds number of 22.6×10^6 reproducing the highest possible Reynolds number during the first wind tunnel test campaign in the ONERA F1. More details on F1 tests can be retrieved in reference [4].

Because during the experiments the flow was forced to be turbulent with the adoption of transition strips on the forefront fuselage and along the full span upper and lower wing surface, thus full turbulent flow conditions on the wing and on the fuselage have been applied in the computations.

RANS equations have been solved with turbulent flow conditions not only on the blocks very close to the solid surface but also on the surrounding nearfield blocks. Euler equations have been solved in the blocks very far from the solid surface (e.g. farfield blocks). Based on the preliminary hypothesis that the flow were attached on the pylon, slip boundary conditions have been applied on its walls. Therefore, only pressure drag could be promptly drawn from the computations while the pylon friction drag contribution has been estimated later on.

Six incidences, 6°, 8°, 10.5°, 10.75°, 11°, 12°, have been run for the wing body configuration while four incidences, 6°, 8°, 10.75°, 12°, for wind tunnel one.

The two-equation Kok TNT $\kappa-\omega$ turbulence model[2, 7] and the multi-grid technique has been adopted for all the computations. Indeed, this turbulence model demostrated its reliability and its capabilities to predict the main feature of this type of vortex flows with respect to alternative turbulence models during the acceptance test exercise[1].

4 Flow solver convergence and runtime

ZEN code convergence history in terms of average residual of conservation mass equation, global lift and drag coefficient, C_L and C_D re-

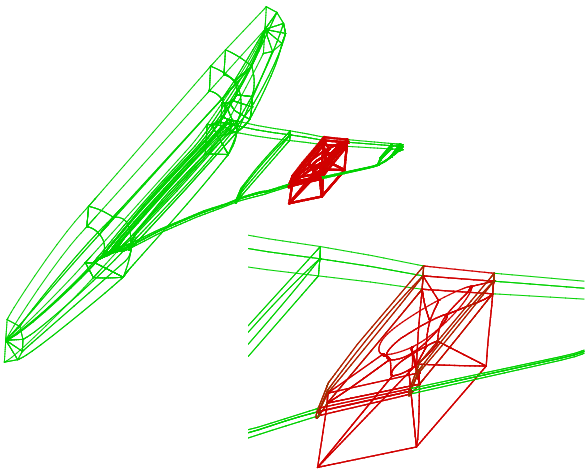

Fig. 6 Grid Topology Modification (red) for the Pylon Inclusion in the Starting Grid

spectively, is shown at wing body configuration design lift in Fig.7 on the three mesh levels. A comparison with the calculation convergence of Wind Tunnel (WT) configuration is also shown.

Calculations converged on both the medium and fine level mesh. The expected global pylon effect (reduced the C_L and increased C_D) has been confirmed. The friction drag coefficient, C_{Df}, not shown here, for the wind tunnel configuration resulted 1 count smaller than the wing body configuration, due to both the slip boundary conditions for the pylon walls and the loss of wetted wing area in the wind tunnel configuration. This result has been found for all the calculated incidences.

Around 10000 iterations were needed to converge the solution on the medium density mesh and around 15000 on the finer level at each incidence.

Taking into account that the multigrid technique has been applied only between two consecutive mesh levels (e.g. on the second level between the second and the first and on the third level between the third and the second but not on the first), the computational times for the wing body configuration ($\sim 4\times10^6$ cells) were the following on the NEC SX-6 supercomputer:

- on the coarse level: 1.77 sec/iter $\times$ 5000 iterations
- on the medium level: 9.96 sec/iter $\times$ 10000 iterations
- on the fine level: 39.03 sec/iter $\times$ 15000 iterations

Therefore, around 8 days have been needed to run a single incidence. The wind tunnel configuration ($\sim 4.25\times10^6$ cells) took a little longer.

5 Aerodynamic coefficient comparison

The comparison between measured and computed global aerodynamic coefficients is commented in this section. The data refer to the up-polar run at the highest Reynolds number in F1 wind tunnel and at the design Mach of 0.25. Indeed, the up-polar runs were considered more reliable if compared with the down-polar counterparts[4]. The WT configuration calculations did not give any pylon friction drag contribution, due to the slip boundary conditions applied on its walls. After the computations the pylon friction drag contribution has been estimated to be around 1 count based on the ratio between the wetted wing and pylon area, under the hypothesis that the flow were attached on the pylon itself. Such hypothesis has been confirmed by experimental evidences by looking at the oil flow visualisation around the pylon area, Fig.8.

The following diagrams include this little correction and the total drag, lift and pitching moment coefficients (subscript *t* in the diagram legend) will be shown together with the breakdown of single component contribution, namely the wing (subscript *w*), the fuselage (subscript *b*) and the pylon (subscript *st*).

Fig.9 shows the lift curve. Due to the adopted drawing scale, it is not easy to appreciate the computed ΔC_L between the wing body and WT configuration but it remains rather constant with the incidence (see the C_L convergence plots in Fig.7). The measured lift curve has been perfectly replicated at lower incidences while at highest incidences some discrepancies have been found. In fact, the non-linearity around the design lift coefficient has been not correctly captured by calculations.

Looking at the drag polar in Fig.10, calculations on wing body configuration highlight overprediction of drag at all the investigated incidences. The overprediction is around 20 counts at the lowest incidence and more than 30 counts at the highest incidence.

The inclusion of the pylon in the computations has allowed to evaluate the influence of model installation in the F1 wind tunnel. Indeed, even if the absolute C_D values are still further off the measured ones, the pylon contribution to drag has been estimated to be $\sim$ 15 counts.

Fig.11 shows the aerodynamic efficiency comparison with a detail around the design C_L in the picture inset. The aerodynamic efficiency data measured on this configuration basically confirm what obtained in the previous experimental campaign on the smaller 1:80 model of

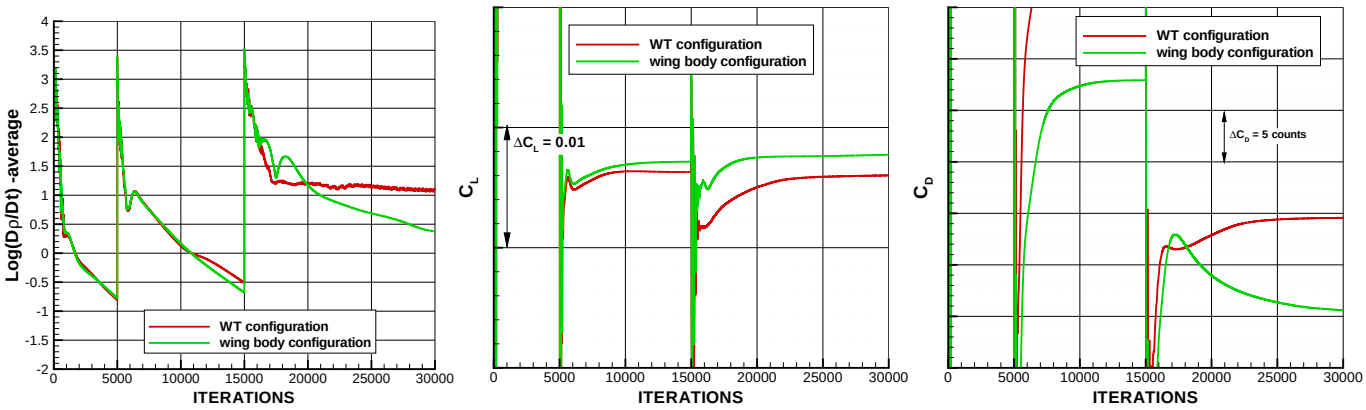

Fig. 7 Convergence history for the wing body and the wind tunnel configuration at design lift: $\alpha = 10.75^\circ$

the EUROSUP configuration[10].

The piching moment curves for the considered configurations are reported in Fig.12. Even if different slope is evident at high incidence between numerical and experimental curve, due to the missing vortex strength on the wing, nevertheless pylon inclusion slightly improves the comparison.

6 Pressure coefficient comparisons

The measured pressure data were available in seven sectional cuts of constant spanwise position.

Four spanwise sections, C1..C4, with tabs all over the chord were on the right wing; further three additional sections, F1..F3, with tabs only on the deflected nose-droop-like leading edge, were on the left wing. Two additional tabs were put on the left wing at C1..C4 position to check the flow symmetry. Not many tabs were put on the lower side of the main wing. Fig.13 gives a description of relative distance between the different sections on the wing. On the lower surface only the sections very close to the pylon are highlighted.

Fig. 8 Oil flow visualisation near the pylon at design lift: $\alpha_{exp} = 10.5^\circ$

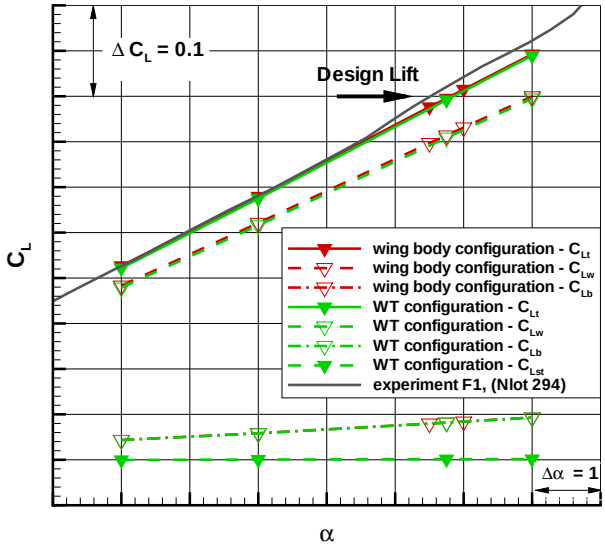

Fig. 9 Comparison of computed and measured lift vs the incidence, M=0.25, Re=22.6×10^6

Here, the comparison between the computed and the measured pressure coefficient, C_p, will only be shown at three spanwise sections, namely C1, C2, and C3, for three selected incidences, namely 8°, 10.75°, which has led to numerical design lift, and 12°; at these incidences both wing

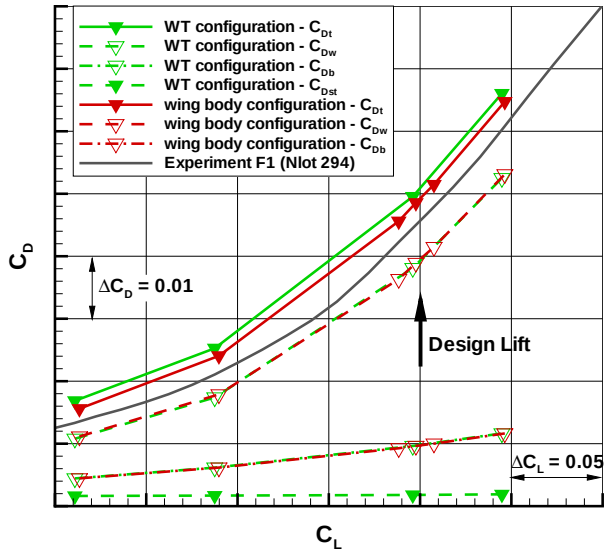

Fig. 10 Comparison of computed and measured drag polar, M=0.25, Re=22.6×10^6

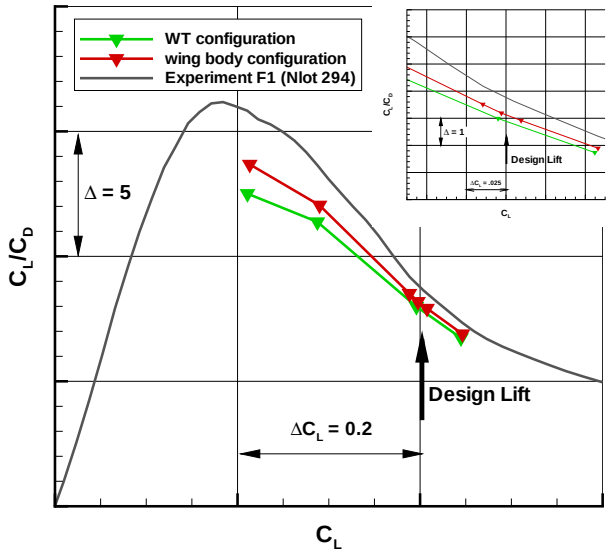

Fig. 11 Comparison of computed and measured aerodynamic efficiency, M=0.25, Re=22.6×10^6

body and WT configuration have been calculated.

Fig.14 shows the comparison at 8°, starting from the inner section, C1, to the outer one, C3. The weak vortex downstream the knuckle on the inner wing is not captured from the simulation, C1 section. A "vortex flap" phenomenon is visible on the upper side along the span, visible from C2 and C3 sections. It leads to a Cp peak between the leading edge and the knuckle position. The most remarkable effect of the pylon on the lower wing is well calculated, C3 section: a compression upward pylon location and a flow acceleration on pylon side. The compression is hardly visible from the experiments due to the lack of pressure tabs in this region. No particular effect of pylon can be observed on the leeward side. Such pylon effect is repeated for all the computed incidences.

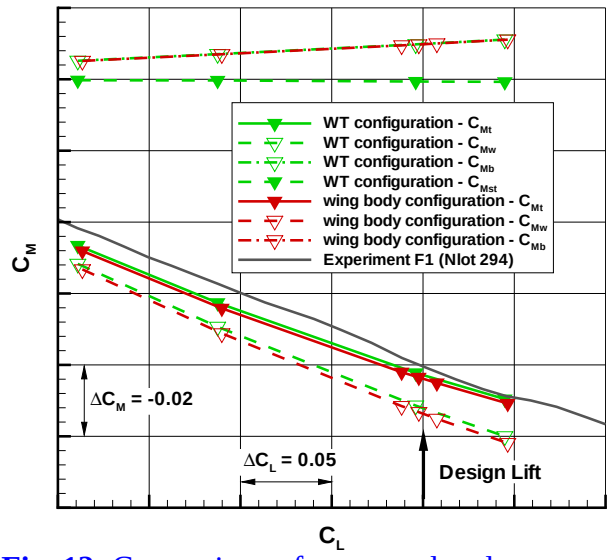

Fig. 12 Comparison of computed and measured piching moment coefficient vs the lift coefficient, M=0.25, Re=22.6×10^6

Fig.15 shows the comparison at 10.75°. C1 section shows that the separation downstream the knuckle suction peak is captured but the extension of vortex flow is more limited in the computation.

The vortex originating from the kink region is quite well captured, C2 section, as well as the more extended separated area on the outer wing along the leading edge. The measurements foresee a more extended separated area well beyond the knuckle position on the outer wing, C3 section. This mismatching between the measured and calculated pressure data can account for the difference in C_L values at the design condition, Fig.9.

At the highest investigated incidence, namely 12°, similar comments as at 10.75° can be repeated. The vortex structure originating from the stub region is well predicted, Fig.16, C1 section, while at the outer sections the measured pressure data are not in good agreement. Indeed, the cal-

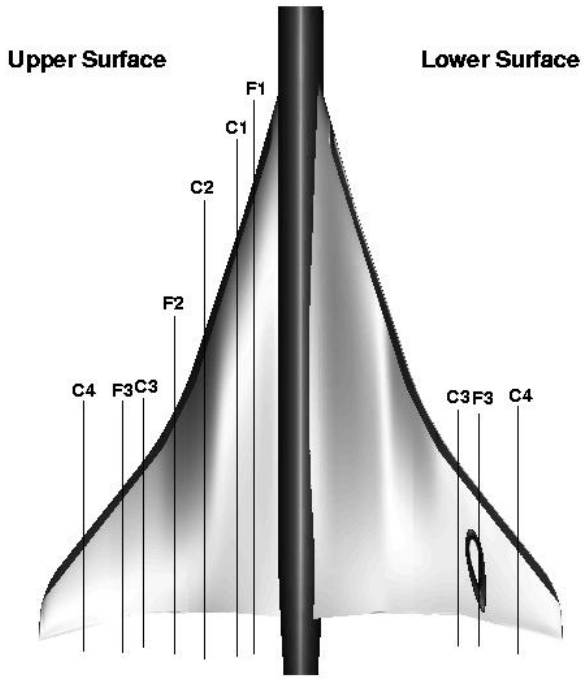

Fig. 13 Wing sections with pressure tabs

culated vortex flow is more confined on the deflected leading edge, with mainly attached flow on the wing beyond the knuckle. In the outer section, C3, the calculated leading edge separation is less than the measured one. The separation in the experiments extends all over the chord.

A possible explanation of the missed separation in the outer sections at the high incidence computations could be that the spatial resolution of wing in spanwise direction around the kink area is too low.

7 Vortex flow development

This section is intended to provide more details on the vortex flow development on the wing. Oil flow visualisations were performed on the three configurations tested during the first experimental campaign, each one at design lift only. Oil flow visualisation was performed on the *"datum"* configuration at 10.5°. This angle of attack led to the design lift for that configuration. Numerical design lift have been reached at higher incidence, namely 10.75°. Therefore, numerical against experimental data will be shown only around the design lift.

Fig.17 shows the computed skin friction line pattern on the upper surface at design C_L compared with the oil flow visualisation counterpart. The calculation predicts a strong vortex along the knuckle with weak vortex flow on the remaining wing surface. On the contrary, the oil flow visualisation clearly highlights the existence of a pair of strong vortices all over the wing originating from the stub and the kink region. This picture mainly confirms that the computed skin friction lines follow the experimental pattern to a certain extent. Fig.18 shows the skin friction line on lower surface with a detail on the pylon area. Skin friction lines could not be computed on the pylon surface because of the assumptions of slip walls during the calculations. The corresponding oil flow visualisation is visible in Fig.8.

The total pressure contour plot on axial cutting planes for the design C_L computation is shown in Fig.19. The weak vortex from the stub region is evident; another contiguous region of total pressure loss is due to the kink vortex which later interacts with the tip vortex. The lift gap at this incidence could be just caused by the underestimation of the vortex flow strength on the wing with respect the experiments. Possible explanations for the missing vortex flow strength on the wing can be the excessive numerical scheme dissipation which dumps vortex spread and/or the lack of spanwise point resolution on the outer wing.

Fig.20 shows the wake pressure loss for the wing body and wind tunnel configuration. The footprint of pylon pressure loss is well evident, especially in the plane just behind the wing.

8 Conclusions

The CIRA RANS flow solver ZEN has been run on a low-speed high-lift SCT configuration. The computations were intended to provide the numerical reference solution to be compared with experimental data collected on a 1:22 scaled model in the ONERA F1 wind tunnel. A streamlined sub-wing pylon has been also included in the computations in order to estimate its effect. Indeed, this pylon stiffened the extremely low-thickness outer wing in order to offset wing tip

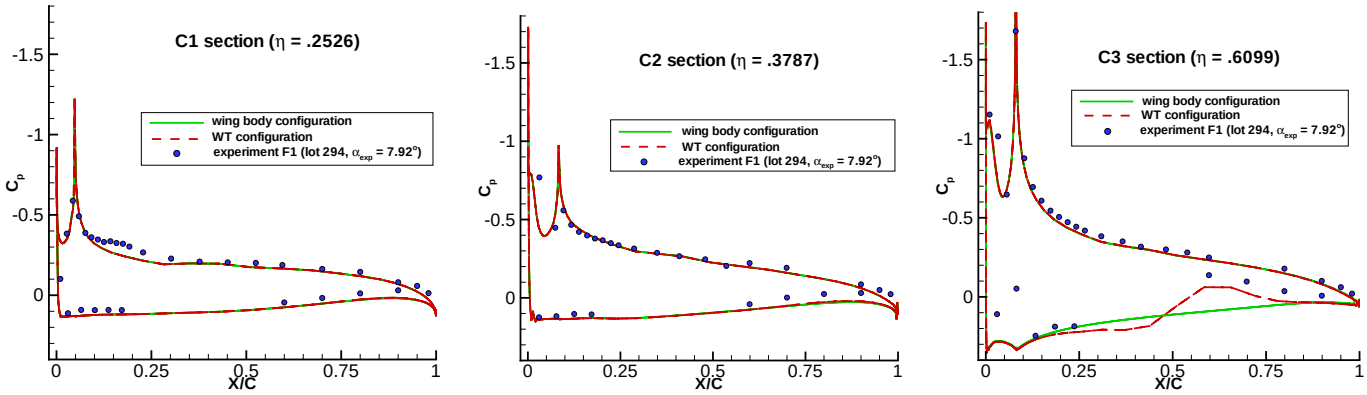

Fig. 14 Comparison between predicted and measured pressure coefficient, $\alpha = 8°$

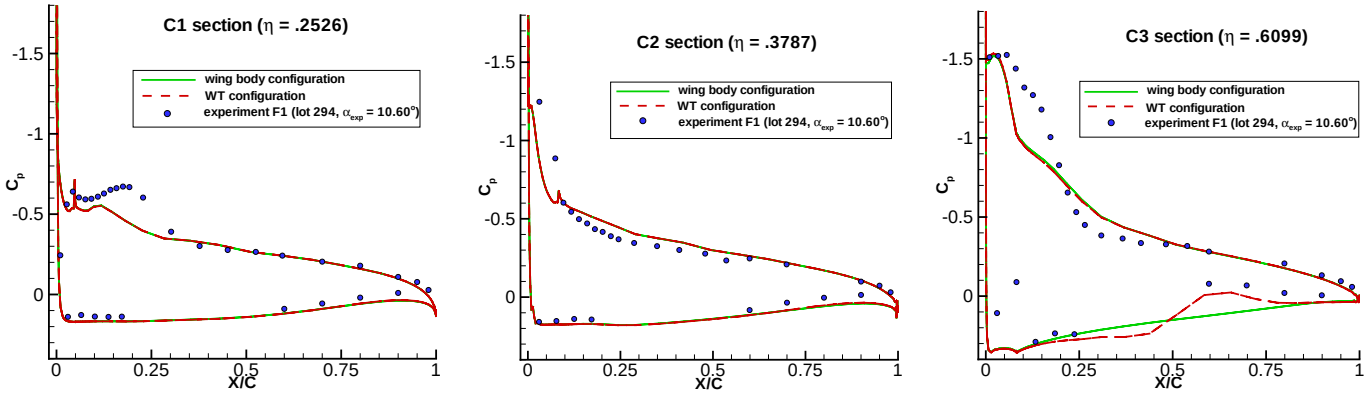

Fig. 15 Comparison between predicted and measured pressure coefficient, $\alpha = 10.75°$

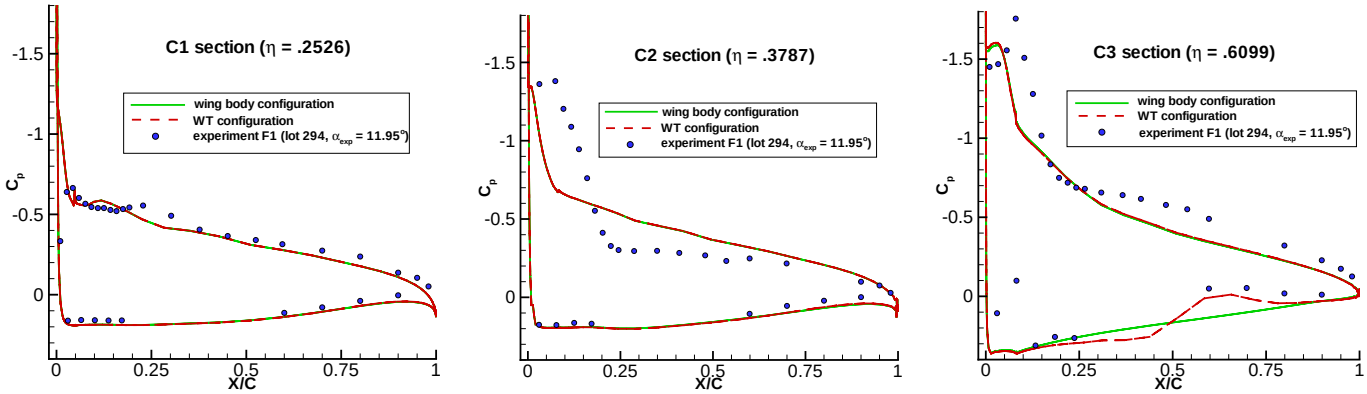

Fig. 16 Comparison between predicted and measured pressure coefficient, $\alpha = 12°$

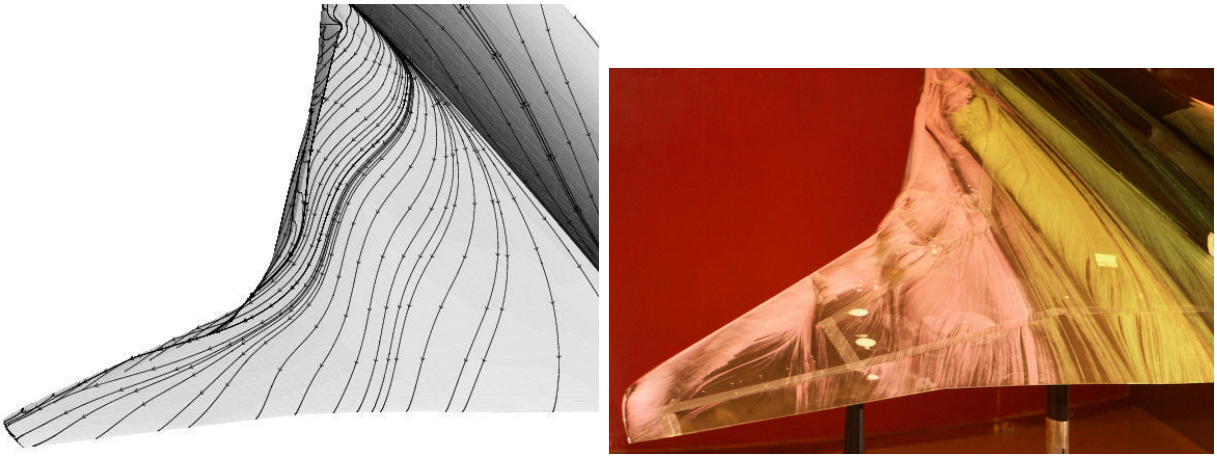

Fig. 17 Skin friction line comparison with oil flow visualization at design lift, M=0.25, Re=22.6×10^6

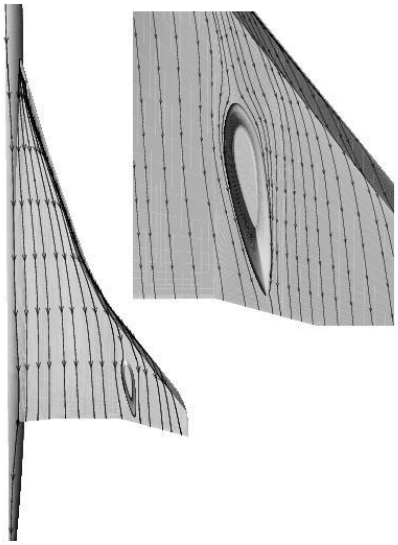

Fig. 18 Skin friction line detail on WT configuration, lower side, M=0.25, Re=22.6×10^6, $\alpha = 10.75°$

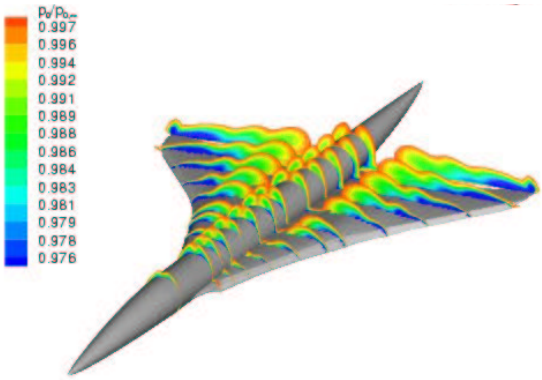

Fig. 19 Total pressure contour plot on axial cutting planes: M=0.25, Re=22.6×10^6, $\alpha = 10.75°$

bending under wind tunnel working conditions. Two grids have been built up around the configurations with minor differences to model the pylon; both have around 4 ×10^6 cells. The Kok TNT $\kappa - \omega$ TM has been used for all the computations. A week of CPU on NEC SX6 has been needed to converge a single angle of attack on the wing body configuration. The wind tunnel configuration has been more difficult to converge especially on the finer mesh level. A general overprediction of the computed drag all over the incidence is the first main finding of such activities. The gap between the experimental data and the calculations increases with the angle of attack ranging from around 20 counts at the lowest incidence until more than 30 counts at the highest incidence. The inclusion of the pylon in the computations has allowed to evaluate the influence of model installation in the F1 wind tunnel on the aerodynamic coefficients. Even if the absolute C_D values are still further off the measured ones, the pylon contribution to drag has been estimated to be around 15 counts. A general agreement of computed and measured lift coefficient is highlighed even if the major vortex lift contribution at the highest incidences is underpredicted by computations. A good agreement is also highlighted by pressure distribution comparison at mainly attached flow conditions. The vortex flow on the deflected leading edge is well predicted at all the incidences while the strong vortex flow which appear on the wing outer sections at the highest incidences is not completely reproduced by computations. This fact accounts for the missed

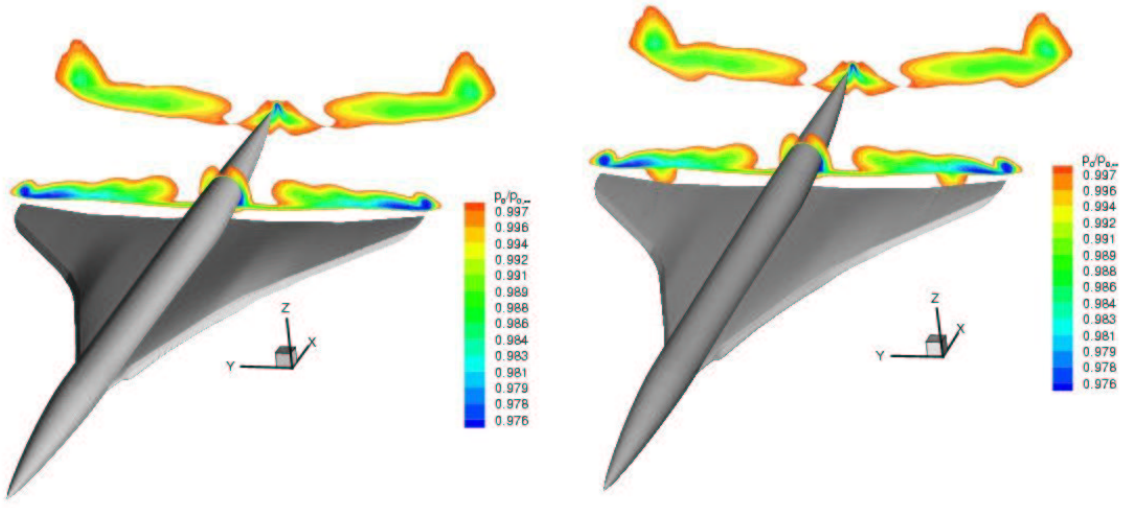

Fig. 20 Total pressure in the wake for the wing body configuration (left) and wind tunnel one (right): M=0.25, Re=22.6×10^6, $\alpha = 10.75°$

lift contribution at high incidences. The major local pylon effect on the lower wing has been well captured. The comparison between the oil flow visualisation and the computed skin friction lines at design condition have highlighted poor agreement on the outer wing sections while the skin friction trend is well replicated on the inner wing. A better refinement of spanwise wing surface grid around the kink area could be a possible solution to the vortex flow resolution on the wing. An excessive numerical scheme dissipation could have also had an additional damping effect on the spread of vortices. Taking into account the intricated flow structures related to this type of configuration, the presented results can be considered very satisfactory.

References

[1] Brandi, V., Amato, M., Catalano, P., *Validation of CIRA flow solver ZEN for SCT low-speed high-lift computations.* 23rd Intern. Congress of the Aeronautical Sciences, September 8-13 2002, Toronto, CA, ICAS-2002-244, 2002.

[2] Catalano P., Amato M., *Assessment of* κ-ω *turbulence modeling in the CIRA flow solver ZEN*. ECCOMAS CFD 2001 Conference, September 4-7 2001, Swansea, Wales, UK

[3] Eggers,Th., *Design Specification of the 1:22 EPISTLE SCT Wind Tunnel Model*. IB 129-2002/3, also EPISTLE-52-DLR-001, February 2002.

[4] Gatard, J., Carrier, G., *EPISTLE 1/22 model tests on 3 strut set-up in F1*. TR 41/03827 DAAP/DSFM, also EPISTLE-6-ONE-007 - February 2004

[5] Herrmann, U., et alii, *Validation of European CFD Codes for SCT Low-Speed High-Lift Computations*. AIAA-Paper No. 2001-2405, 2001.

[6] Herrmann, U., *Low Speed High-Lift Perfomance Improvement obtained and Validated by EC-Project EPISTLE*. 24th International Congress of the Aeronautical Sciences, August 29 - September 3, Yokohama, Japan, ICAS-2004-411, 2004.

[7] Kok J. C., *Resolving the dependence on free-stream values for the* κ-ω *turbulence model*. *AIAA Journal*, Vol. 38, n. 7, July 2000, pp. 1292-1295

[8] Kok J. C., Amato M., Boerstoel J. W., *Mathematical-Physical modeling for multi-block NaS/Euler simulation*. CIRA-DLCEST-TR183, and NLR-CR91-235L

[9] Lovell, D.A., *European research of wave and lift dependent drag for Supersonic Transport Aircraft*. AIAA-Paper No. 99-3100, 1999.

[10] Rohne, P.B., Hoolhorst A. and Goossens J.D., *Data Report on Low Speed Measurements in the HST for the EPISTLE Project*. DNW-ASD-2000-032, 2000.